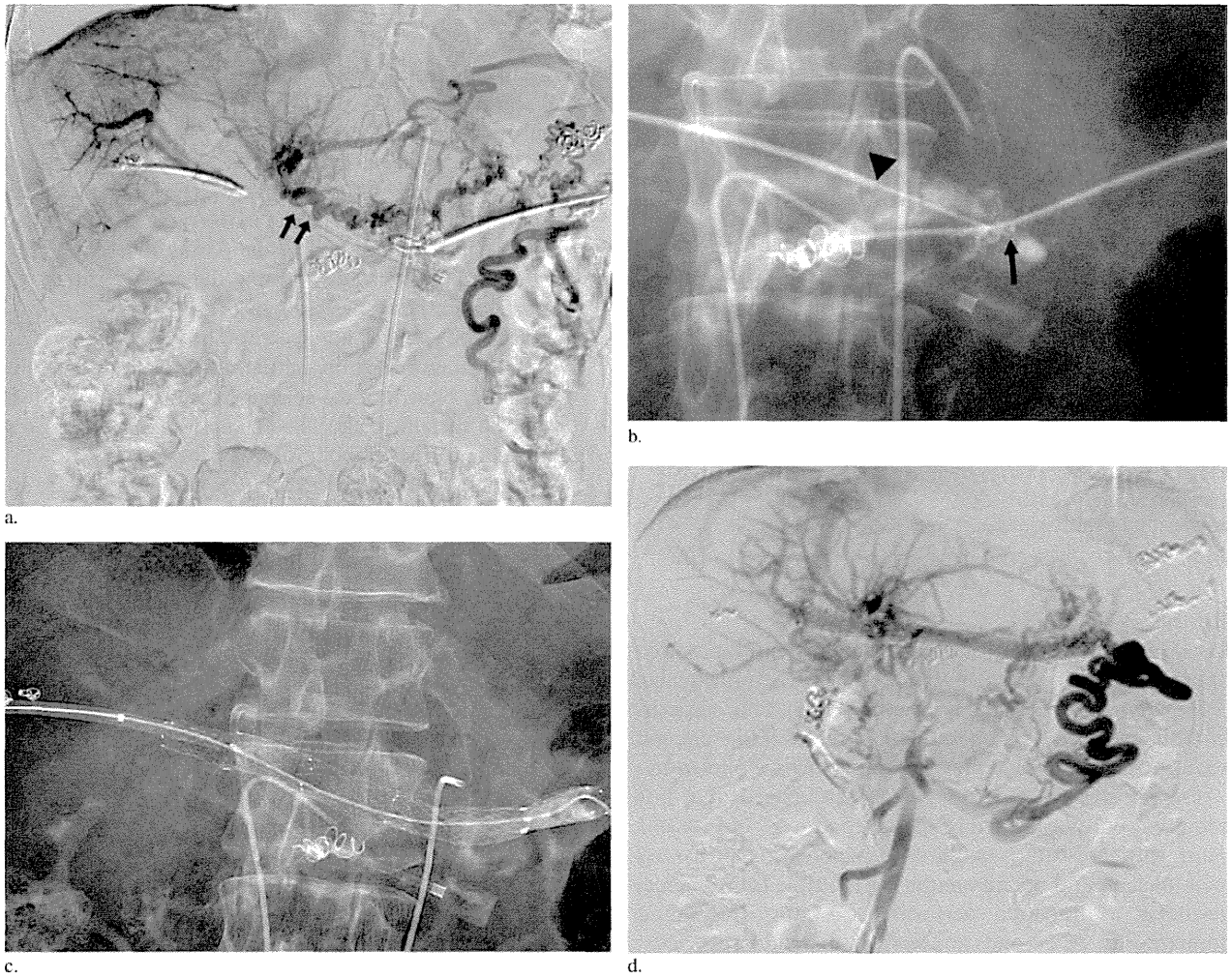

Figure 2. Technical steps of the creation of an extraanatomic splenoportal shunt. **(a)** Transhepatic portography and simultaneous transsplenic splenic venography. Occlusion of splenic vein and portal vein with collateral vessels forming (arrows) are demonstrated. Catheters in the aorta and vena cava, placed in case of massive bleeding, are seen. **(b)** Coaxial technique was employed to puncture the splenic vein from the right portal vein. A 17-gauge needle was advanced to the occlusion point of the portal vein (arrowhead), and the splenic vein was successfully punctured with a 21-gauge needle (arrow) from the 17-gauge needle. **(c)** Two covered stents and two bare metal stents were deployed, traversing the extraanatomic shunt route between the right portal and splenic veins. **(d)** Mesenteric venography after the third procedure. Stents in a TIPS route placed between the right hepatic and right portal veins during the second procedure are seen. Residual varices were embolized. Both bypass route and intrahepatic portal veins are patent.

to maintain the flow in the branch vessels. Balloon angioplasty was performed to dilate the unexpanded stents with a 10-mm × 4-cm balloon catheter (PowerFlex P3; Cordis, Bridgewater, New Jersey). As stagnation in the stents was seen, presumably as a result of insufficient outflow from the splenoportal shunt, a TIPS was created between the right hepatic and right portal veins with the use of a Rösch–Uchida Transjugular Liver Access Set (Cook) and an 8-mm × 4-cm bare metal stent (Zilver). Percutaneous catheters were removed, and tract embolization was performed.

After the procedure, bleeding decreased significantly; however, a small amount of melena with mild anemia was observed and residual varices were seen on CT. Therefore, embolization of the residual varices with n-butyl-2-cyanoacrylate (Histoacryl; B. Braun, Bethlehem, Pennsylvania) and Lipiodol (B. Braun) mixed at a 1:6 ratio was performed from the surgically exposed ileocecal vein 20 days after creation of the splenoportal shunt (Fig 2d). After these procedures, the variceal bleeding was stopped and transfusions were no longer required. Endoscopy and CT demonstrated the shrinkage of varices. Contrast-enhanced CT (Fig 3) and Doppler US at 10 and 12 months demonstrated patent splenoportal and portosystemic shunts. No anticoagulants were administered. The patient has remained well, without episodes of variceal bleeding at 14 months after the procedures.

Ectopic varices arising in the small intestine are often inaccessible by an endoscope. Therefore, the diagnosis and

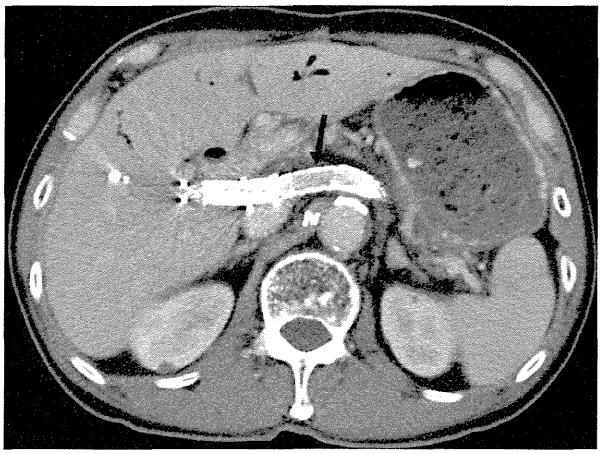

Figure 3. Axial contrast-enhanced CT at 10 months after the procedure. Stents in the splenoportal shunt are patent (arrow) and varices are decreased in size.

treatment methods are determined on a case-by-case basis. A 2013 literature review by Saeki et al (1) identified 13 cases, from 11 reports, of bleeding ectopic varices at the sites of previous choledochojejunostomies. In that series, interventional radiologic techniques were employed in eight patients, including dilation and stent implantation of the portal vein (n = 5) and embolization of varices (n = 3). None of these cases involved percutaneous creation of an extraanatomic shunt as performed in the present case. Decompression of splenic outflow with an extraanatomic shunt was effectively established in the patient described here; however, attempts at recanalization of the portal and splenic veins may have caused fatal complications such as massive abdominal bleeding and should be considered carefully.

Transsplenic access to the splenic vein in patients with an occluded portal vein is a recognized technique (2,3). Because bleeding from the soft and fragile spleen could be a lethal complication, embolization of the puncture tract should be performed. In the present case, both transsplenic approach sessions were uneventful with tract embolization. In addition, successful recanalization of occluded portal veins via a transsplenic approach has been reported (2,3) as in the present case.

In summary, the present case illustrates extraanatomic splenoportal shunt creation in a patient with bleeding jejunal varices after a choledochojejunostomy. This technique may serve as a treatment option for patients with ectopic varices caused by extrahepatic portal venous occlusion associated with difficult portal vein recanalization.

REFERENCES

1. Saeki Y, Ide K, Kakizawa H, Ishikawa M, Tashiro H, Ohdan H. Controlling the bleeding of jejunal varices formed at the site of choledochojejunostomy: report of 2 cases and a review of the literature. Surg Today 2013; 43:550–555.
2. Zhu K, Meng X, Zhou B, et al. Percutaneous transsplenic portal vein catheterization: technical procedures, safety, and clinical applications. J Vasc Interv Radiol 2013; 24:518–527.
3. Tuite DJ, Rehman J, Davies MH, Patel JV, Nicholson AA, Kessel DO. Percutaneous transsplenic access in the management of bleeding varices from chronic portal vein thrombosis. J Vasc Interv Radiol 2007; 18:1571–1575.

Imagine IR Symposium: An Approach to Increasing IR Awareness and Understanding among Medical Students

From: Prasaanthan Gopee-Ramanan, BSc (Hons)
Tyler Michael Coupal, MD
Jason Martin, MD
Jatin Kaicker, MD
Sandra Reis Welsh, MRT(R)
Sriharsha Athreya, MS, FRCS, FRCR
Michael G. DeGroote School of Medicine (P.G.R., T.M.C., J.M., J.K.)
McMaster University
Hamilton, Ontario, Canada; and
Diagnostic Imaging Department (S.R.W., S.A.)
St. Joseph's Healthcare Hamilton
50 Charlton Ave. E
Hamilton, ON, Canada L8N 4A6

Editor:

Throughout the past decade, academic literature has repeatedly reported high levels of interest in interventional radiology among medical students; however, it has been shown that students continue to have a limited understanding of interventional radiology concepts and its scope of practice (1). Of 103 responses from 542 medical students surveyed from a Canadian university's medical program, a total of 18% reported being interested in interventional radiology as a career, but 54% of students were unclear about the duties of an interventional radiologist in the hospital (1). Moreover, nearly 75% of students expressed concerns with regard to limited interventional radiology exposure and supported a proposed mandatory interventional radiology rotation (1). Although this supports the notion that new approaches to interventional radiology education are required, current academic literature has not identified effective and practical means of approaching interventional radiology education.

An evening symposium entitled Imagine IR 2.0 was implemented in October 2013 and included small-group workshops and problem-based learning sessions aimed at introducing the subspecialty of interventional radiology to undergraduate medical students. Short lectures and hands-on demonstrations were also elements of the program. The event was a collaborative and interprofessional undertaking by interventional radiologists, a radiological technologist, and a diagnostic imaging

None of the authors have identified a conflict of interest.

http://dx.doi.org/10.1016/j.jvir.2014.03.011

Two Esophageal Stents in the Abdomen

Shinichi Morita, MD, Yasuaki Arai, MD, and Miyuki Sone, MD

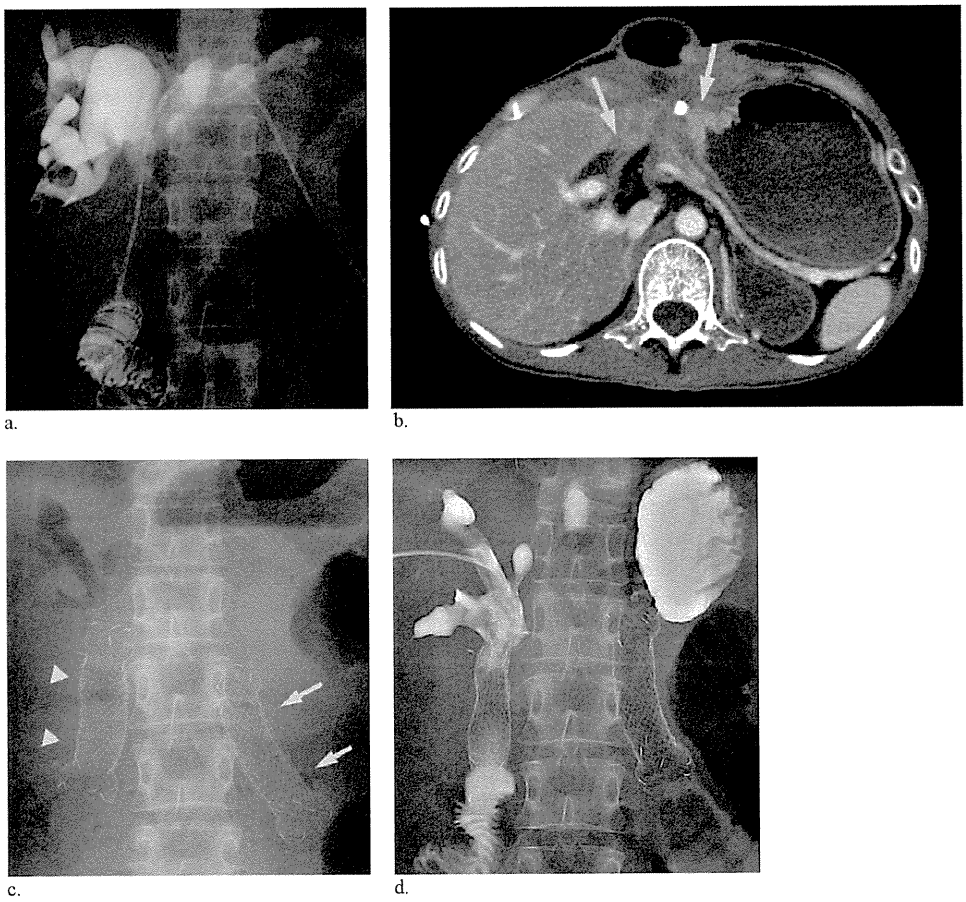

Figure.

A 32-year-old woman presenting with frequent vomiting and jaundice was referred to our hospital. Twelve years previously, she had been diagnosed with cholangiocarcinoma associated with congenital bile duct dilation (Fig a, shows preoperative cholangiography). At that time, the extrahepatic bile duct was resected, and gastrojejunostomy was performed. Computed tomography revealed obstruction of the choledochojejunostomy and gastrojejunostomy anastomotic sites by recurrent tumors (Fig b, arrows). An esophageal self-expandable silicon-covered metallic stent—with a wide aperture and flared structures at both ends to prevent stent migration—was placed percutaneously to relieve biliary obstruction (Fig c, arrowheads). To improve food passage, the same type of stent was placed via her mouth at the gastrojejunostomy stricture (Fig c, arrows). The jaundice and vomiting improved following stent placement (Fig d). Both stents were functioning 10 months later, and she has remained well. Metallic stents are designed for use in multiple anatomic locations. Proper metallic stent selection and placement can dramatically ameliorate symptoms.

From the Department of Diagnostic Radiology, National Cancer Center Hospital, 5-1-1 Tsukiji, Chuo-ku, Tokyo 1040045, Japan. Received April 22, 2014; final revision received and accepted April 26, 2014. **Address correspondence to** S.M.; E-mail: m0riz0u@extra.ocn.ne.jp

None of the authors have identified a conflict of interest.

J Vasc Interv Radiol 2014; 25:1193

http://dx.doi.org/10.1016/j.jvir.2014.04.022

Radiotherapy and Oncology 113 (2014) 193–197

Contents lists available at ScienceDirect

Radiotherapy and Oncology

journal homepage: www.thegreenjournal.com

PET/CT in head and neck cancer

Correlation of ^{18}F-BPA and ^{18}F-FDG uptake in head and neck cancers

Hitomi Tani [a,c], Hiroaki Kurihara [a,*], Kenta Hiroi [a], Natsuki Honda [a], Mitsuyoshi Yoshimoto [b], Yuzuru Kono [a], Ryusuke Murakami [c], Shinichiro Kumita [c], Yasuaki Arai [a], Jun Itami [d]

[a] Department of Diagnostic Radiology, National Cancer Center Hospital, Tokyo; [b] Division of Functional Imaging, National Cancer Center Hospital East, Chiba; [c] Department of Radiology, Nippon Medical School, Tokyo; and [d] Department of Radiation Oncology, National Cancer Center Hospital, Tokyo, Japan

ARTICLE INFO

Article history:
Received 29 May 2014
Received in revised form 16 October 2014
Accepted 1 November 2014
Available online 18 November 2014

Keywords:
BPA
FDG
PET/CT
Head and neck tumor
BNCT

ABSTRACT

Background and purpose: The aim of this study was to compare the accumulation of 4-borono-2-^{18}F-fluoro-phenylalanine (^{18}F-BPA) with that of ^{18}F-fluorodeoxyglucose (^{18}F-FDG) in head and neck cancers, and to assess the usefulness of ^{18}F-FDG PET for screening candidates for boron neutron capture therapy (BNCT).

Material and methods: Twenty patients with pathologically proven malignant tumors of the head and neck were recruited from March 2012 to January 2014. All patients underwent both whole-body ^{18}F-BPA PET/CT and ^{18}F-FDG PET/CT within 2 weeks of each other. The uptakes of ^{18}F-BPA and ^{18}F-FDG at 1 h after injection were evaluated using the maximum standardized uptake value (SUVmax).

Results: The accumulation of ^{18}F-FDG was significantly correlated with that of ^{18}F-BPA. The SUVmax of ^{18}F-FDG $\geqslant$5.0 is considered to be suggestive of high ^{18}F-BPA accumulation.

Conclusions: ^{18}F-FDG PET might be an effective screening method performed prior to ^{18}F-BPA for selecting patients with head and neck cancer for treatment with BNCT.

 Radiotherapy and Oncology 113 (2014) 193–197

Boron neutron capture therapy (BNCT) is a targeted radiotherapy technique developed to treat patients with selected malignant tumors. It has been tested in brain *tumors*, head and neck cancers and melanoma which are radioresistant with infiltrative growth pattern [1–4].

This particular radiation therapy is based on the combined use of thermal neutrons and one of the two stable isotopes of boron (^{10}B) to destroy tumor cells via the ^{10}B$(n,\alpha)^{7}$Li neutron capture reaction. Thermal neutrons cause the boron neutron capture reaction. Epithermal neutrons are slowed down in the body and are especially needed if deep seated tumors are intended to be treated. It requires a high-intensity epithermal neutron beam and a ^{10}B carrier that accumulates in target tumor cells. Interaction of neutrons with ^{10}B nuclei releases alpha particles and recoiling lithium-7 nuclei with very short range (<10 μm) that should kill the cell. The selectivity of the therapy is based on the fact that only tumor cells containing ^{10}B are destroyed, preserving normal tissues due to their low affinity for the boron drug [1,2,5]. The success of BNCT is dependent on the sufficient accumulation of ^{10}B in cancer tissue relative to adjacent tissues, with preferably a 3- to 5-fold greater concentration in the former [1,2]. Therefore, estimation of ^{10}B content in tumor and normal tissue helps predict the therapeutic potential of BNCT. Since ^{10}B accumulation varies by tumor type, and even tumors of the same grade may differ in their biochemical properties, it would be highly desirable to determine ^{10}B concentrations prior to performing BNCT.

The most frequently used ^{10}B carrier compound today is 4-^{10}B-borono-L-phenylalanine (^{10}BPA). An ^{18}F-labeled analog of ^{10}BPA, 4-borono-2-^{18}F-fluoro-phenylalanine (^{18}F-BPA) has been developed to predict ^{10}B concentrations in tumors [6]. Imahori et al. designed a method for quantitative measurement of ^{10}B concentrations using ^{18}F-BPA positron emission tomography (PET) [7,8]. ^{18}F-BPA PET is generally used to anticipate the therapeutic effects of BNCT performed using ^{10}BPA [5–9]. However, only certain hospitals have the capability to synthesize ^{18}F-BPA [9]. Synthesis of ^{18}F-BPA from $^{18}F_2$ gas is limited because of low radio yield, low specific activity, and high cost. Therefore, the amount of ^{18}F-BPA, which can reasonably be synthesized is not sufficient to screen all potential BNCT candidates. Because of these limitations, it is often not easy to assay the ^{10}B concentrations in tumor and normal tissues using ^{18}F-BPA PET.

^{18}F-fluorodeoxyglucose (^{18}F-FDG) is the most popular PET tracer and is available in many hospitals. ^{18}F-FDG PET is a highly sensitive tool capable of yielding considerable information on glucose metabolism [10]. It has been used in the assessment of various cancers, as several malignant tumors consume large amounts of glucose [11]. The use of ^{18}F-FDG PET as a surrogate marker for ^{18}F-BPA could have wider applicability. Thus far no reports have directly compared ^{18}F-FDG with ^{18}F-BPA.

* Corresponding author.
E-mail address: hikuriha@ncc.go.jp (H. Kurihara).

http://dx.doi.org/10.1016/j.radonc.2014.11.001
0167-8140/

Though the majority of patients undergoing BNCT have brain tumors such as high-grade gliomas and cerebral metastasis [1,2], the role of ^{18}F-FDG in brain tumors is limited because of high gray matter uptake. Recently, however, use of BNCT has extended to head and neck cancers [12–14]. In this study, we used PET to examine the uptake of both ^{18}F-BPA and ^{18}F-FDG in head and neck cancers. Our aim was to compare the accumulation of ^{18}F-BPA with that of ^{18}F-FDG in head and neck cancers, and to evaluate the usefulness of ^{18}F-FDG PET for screening potential candidates for BNCT.

Materials and methods

General

All chemical reagents were obtained from commercial sources. The study protocol was approved by the institutional review board and independent ethics committee of our hospital. All patients signed written informed consent before inclusion in the trial.

Subjects

Patients included in this study had histologically confirmed head and neck tumors, at least 1 site of disease measurable via PET, Eastern Cooperative Oncology Group performance status (PS) of 0–1, adequate organ function (neutrophil count $\geqslant$1500/μL, platelet count $\geqslant$75,000/μL, hemoglobin concentration $\geqslant$9.0 g/dL, serum bilirubin $\leqslant$1.5 mg/dL, AST and ALT $\leqslant$100 IU/L, serum creatinine $\leqslant$1.5 mg/dL, baseline left ventricular ejection fraction (LVEF) >60%), and were over 20 years old. The main exclusion criteria were congestive heart failure, uncontrolled angina pectoris, arrhythmia, symptomatic infectious disease, severe bleeding, pulmonary fibrosis, obstructive bowel disease or severe diarrhea, and symptomatic peripheral or cardiac effusion.

Radiosynthesis of ^{18}F-BPA and ^{18}F-FDG

^{18}F-BPA was synthesized by direct electrophilic radiofluorination of BPA (Sigma–Aldrich, St. Louis, MO, USA) using ^{18}F-acetyl hypofluorite as described previously [15]. Purification of ^{18}F-BPA was performed by HPLC using a YMC-Pack ODS-A column (20 × 150 mm; YMC, Kyoto, Japan) eluted with 0.1% acetic acid at a flow rate of 10 mL/min. The radiochemical purity of ^{18}F-BPA, determined by HPLC, was >99.5%, and its specific activity was 25 MBq/μmol. ^{18}F-FDG was prepared using an automated ^{18}F-FDG-synthesis system (F-200, Sumitomo Heavy Industries, Ltd.).

PET/CT scanner and protocol

The examination schedule is shown in Fig. 1. Images were acquired with Discovery 600 scanner (GE Healthcare, Milwaukee, WI, USA). A whole-body ^{18}F-FDG PET/CT image was obtained 1 h after the injection of ^{18}F-FDG (ca. 4 MBq/kg). For the ^{18}F-FDG PET/CT studies, patients were requested to fast for at least 4 h before the scheduled ^{18}F-FDG injection. Whole-body ^{18}F-BPA PET/CT imaging was also carried out within 2 weeks. ^{18}F-BPA PET/CT images were acquired 1 h after the injection of ^{18}F-BPA (ca. 4 MBq/kg).

For whole-body PET/CT imaging, a scout image was acquired to determine the scanning field ranging from head to pelvis, using settings of 10 mA and 120 kV. Next, whole-body 16-slice helical computed tomography (CT) and whole-body 3D PET were performed. PET images were acquired in 7–8 bed positions with a 2 min acquisition period per bed position, so that the imaging covered the same field as that of whole-body CT. The acquired data were reconstructed as 192 × 192 matrix images (3.65 × 3.65 mm) using a 3D ordered subsets-expectation maximization (3D OS-EM) algorithm.

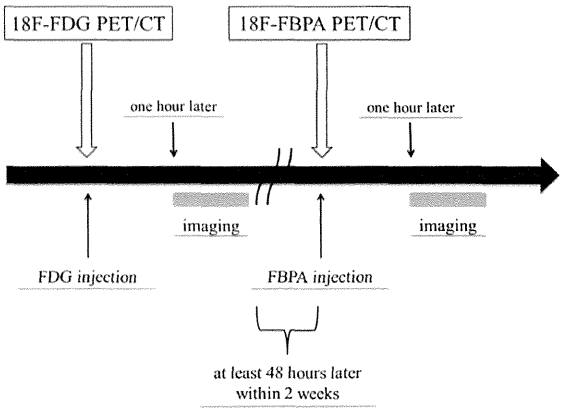

Fig. 1. Schedule of PET/CT examinations.

Tumor uptake of ^{18}F-BPA and ^{18}F-FDG

PET image evaluation and quantification of the standardized uptake value (SUV) were performed using AW Volume Share 4.5 software (GE Healthcare, Milwaukee, WI, USA). Regions of interest (ROIs) were delineated on the PET/CT images, and the maximum SUV in each ROI (SUVmax) was determined. Tumor ROIs were defined as the areas of highest activity. SUV was defined as the regional radioactivity divided by the injected radioactivity normalized to the body weight. Both the ^{18}F-BPA and ^{18}F-FDG uptake 1 h after injection were evaluated using SUVmax. At the corresponding level on ^{18}F-BPA PET, ROIs were then placed onto the normal tissue region surrounding the tumor to calculate the lesion to normal ratio (L/N) of ^{18}F-BPA. Clinically, dose planning was performed based on L/N ratio prior to initiation of BNCT. Tumor sizes were also measured on CT.

Statistical analysis

A linear regression analysis was performed for the correlation study. As previously reported, patients were determined eligible for BNCT when the L/N ratio of ^{18}F-BPA was more than 2.5 [1,8,16], so we used a L/N ratio of ^{18}F-BPA $\geqslant$2.5 to differentiate positive from negative. We then performed a receiver operating characteristic (ROC) analysis for SUVmax of ^{18}F-FDG to determine the optimal threshold values for quantitative discrimination. The area under the curve (AUC) was also calculated. For estimating concordance of cutoff value of the 2 tracers, Fisher's exact test was performed. Probability values of $P < 0.05$ were considered significant.

Results

Patient and tumor characteristics are summarized in Table 1. A total of 20 patients (17 male, 3 female, age range 30–76 years, mean age 62 years) with pathologically proven head and neck malignant tumors were enrolled in this study from March 2012 to January 2014. All patients had unresectable advanced or recurrent head and neck tumors. The majority of primary tumor sites were the pharynx or parotid gland. Tumor histological types varied: 9 patients had squamous cell carcinoma, 5 had adenoid cystic carcinoma and the remaining 6 had other types of malignant tumors. Fourteen of the 20 patients had local recurrent tumors, 5 had metastatic tumors and one had a newly diagnosed tumor.

Typical PET/CT images of ^{18}F-BPA and ^{18}F-FDG are shown in Fig. 2. SUVmax and L/N ratio of ^{18}F-BPA, SUVmax of ^{18}F-FDG and measured tumor size are summarized in Table 1. The tumor SUVmax of ^{18}F-BPA ranged from 1.79 to 8.19 (average, 4.13), whereas

Table 1
Patient and tumor characteristics.

	Gender	Age	Location of primary tumor	Histology	Prior therapy	Disease presentation	FBPA SUVmax	FBPA L/N ratio	FDG SUVmax	Size (mm × mm)
1	M	75	Gingiva	Squamous cell carcinoma	Postop/RT	Local recurrence	3.85	2.69	7.40	61 × 35
2	M	76	Epipharynx	Squamous cell carcinoma	RT	Local recurrence	7.05	5.78	12.30	42 × 21
3	F	30	Parotid gland	Adenoid cystic carcinoma	RT	Local recurrence	3.70	2.94	9.90	64 × 53
4	M	63	Maxillary sinus	Adenoid cystic carcinoma	RT	Local recurrence	1.79	1.35	1.90	24 × 10
5	M	57	Oropharynx	Squamous cell carcinoma	CRT	Local recurrence	5.23	4.63	15.60	47 × 23
6	M	72	Palpebra	Basal cell carcinoma	CRT	Local recurrence	3.46	2.70	9.80	67 × 26
7	M	65	Hypopharynx	Squamous cell carcinoma	CRT	LN metastasis	8.19	5.98	12.70	48 × 44
8	M	46	Epipharynx	Neuroendocrine cell carcinoma	CRT	LN metastasis	4.06	3.44	8.50	27 × 22
9	M	61	Parotid gland	Adenoid cystic carcinoma	Postop/RT	LN metastasis	3.92	3.11	12.00	68 × 41
10	M	61	Maxillary sinus	Adenocarcinoma	Postop/CRT	Local recurrence	1.99	1.75	4.40	11 × 11
11	M	75	Elbow skin	Adenoid cystic carcinoma	Postop	Parotid gland metastasis	3.32	2.53	5.10	19 × 16
12	F	70	Hypopharynx	Squamous cell carcinoma	CRT	Local recurrence	2.00	1.43	4.60	12 × 11
13	M	66	Maxillary sinus	SQUAMOUS cell carcinoma	Postop/CRT	Local recurrence	5.09	4.21	20.71	59 × 27
14	M	66	Hypopharynx	Squamous cell carcinoma	CRT	Local recurrence	6.78	4.08	14.10	33 × 22
15	M	63	Oropharynx	Squamous cell carcinoma	Postop/CRT	Local recurrence	3.15	2.58	9.83	23 × 15
16	M	47	Parotid gland	Salivary duct carcinoma	Postop	Local recurrence	5.56	4.71	11.55	37 × 29
17	F	66	Parotid gland	Pleomorphic adenoma	Postop	Local recurrence	5.78	4.48	5.01	38 × 32
18	M	69	Oral cavity	Adenoid cystic carcinoma	No	Newly diagnosed tumor	2.81	2.27	10.44	41 × 32
19	M	47	Nasal cavity	Esthesioneuroblastoma	RT	LN metastasis	3.19	2.17	9.94	36 × 19
20	M	68	Oropharynx	Squamous cell carcinoma	CRT	Local recurrence	1.82	1.54	2.26	28 × 11

Abbreviations: Postop = postoperative; RT = radiotherapy; CRT = chemoradiation therapy; LN = lymph node.

Fig. 2. Typical ^{18}F-BPA and ^{18}F-FDG PET/CT images at 1 h after injection (Patient No. 5: 75 year-old man with epipharyngeal carcinoma). A: ^{18}F-BPA PET/CT image at 1 h after injection (SUVmax = 7.1). B: ^{18}F-FDG PET/CT image at 1 h after injection (SUVmax = 11.8). Upper panel: maximum intensity projection image; lower panel: PET/CT fusion image.

that of ^{18}F-FDG ranged from 1.90 to 20.71 (average, 9.40). In 19 of 20 cases, the SUVmax of ^{18}F-FDG was higher than that of ^{18}F-BPA. A significant correlation was observed between uptake of ^{18}F-BPA and ^{18}F-FDG (Fig. 3; $r = 0.72$, $P < 0.01$). ROC analysis revealed that the AUC of SUVmax of ^{18}F-FDG was 0.87 and the cutoff value was 5.01 (Fig. 4). We then determined positive and negative uptake of ^{18}F-BPA and ^{18}F-FDG using the following cutoffs: an L/N ratio of ^{18}F-BPA $\geqslant$2.5 and an SUVmax of ^{18}F-FDG $\geqslant$5.0. With these parameters, 14 patients were classified as positive for both ^{18}F-BPA and ^{18}F-FDG, 4 were negative both for ^{18}F-BPA and ^{18}F-FDG, and 2 were positive for ^{18}F-FDG and negative for ^{18}F-BPA. The association between the positive/negative classifications of ^{18}F-FDG and ^{18}F-BPA was statistically significant (Fisher exact test, $P < 0.01$).

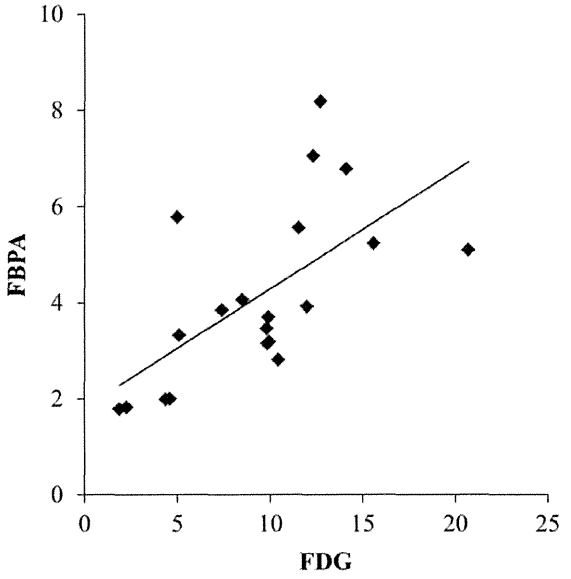

Fig. 3. Relationship between ^{18}F-BPA uptake and ^{18}F-FDG uptake in 20 head and neck cancers. A significant correlation was observed between ^{18}F-BPA uptake and ^{18}F-FDG uptake ($r = 0.72$, $P < 0.01$).

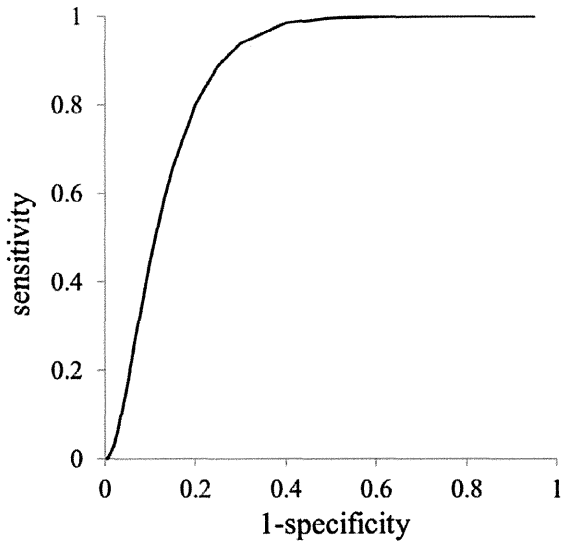

Fig. 4. ROC analysis of SUVmax of ^{18}F-FDG when the L/N ratio of ^{18}F-BPA $\geqslant$2.5 was used. The AUC of SUVmax of ^{18}F-FDG was 0.87 and the cutoff value was 5.01.

Discussion

Used with a variety of tracers and a multidisciplinary approach, PET can provide qualitative and quantitative data to serve as a prognostic and therapeutic indicator. The aim of this study was to compare the accumulation of ^{18}F-BPA and ^{18}F-FDG in head and neck cancers and to assess the usefulness of ^{18}F-FDG PET for screening BNCT candidates. A significant correlation between ^{18}F-BPA and ^{18}F-FDG tumor uptake was observed in head and neck cancers. Our results suggested that an SUVmax of ^{18}F-FDG $\geqslant$5.0 is considered to be the optimal threshold value for prediction of an L/N ratio of ^{18}F-BPA $\geqslant$2.5.

^{18}F-BPA is an amino acid PET tracer, while ^{18}F-FDG is a known tracer of glycolysis [9–10]. While the mechanism of ^{18}F-BPA accumulation is thought to depend on amino acid transport systems, there are few reports on the in vivo kinetics of ^{18}F-BPA derivatives in tumors. A previous study reported that ^{18}F-BPA is a system L-specific imaging agent [9]. System L is a primary contributor to ^{18}F-BPA uptake; this uptake correlates with total L-amino acid transporter (LAT) expression but more specifically with that of LAT1 and LAT4. Many tumors overexpress LAT1 or LAT4 [17–19], and phenylalanine is a substrate for both of these [20].

In contrast to ^{18}F-BPA, ^{18}F-FDG has been used to measure glucose metabolism in vivo, and is taken up and retained by cancer cells because of the presence of glucose transporters (glut-1) and other molecules [10]. High ^{18}F-FDG uptake in tumor cells has been reported to reflect increased activity of either glucose transport or hexokinase [21] and to correlate with tumor growth rates [22] and cell density [23].

Though the accumulation mechanisms of these 2 tracers are different in vitro, tumor uptake of both molecules is thought to be associated with the viability of cancer cells in vitro and that of tumor tissue in vivo. Correlation between the uptake of ^{18}F-BPA and ^{18}F-FDG might be due to factors such as proliferation, metabolic activity, viability of tumor cells, and cell density within the tumor. However, these are hypothetical factors and not proved in this study. Further studies are needed for correlation between the histopathologic examination and uptake of both tracers.

In this study, we found that ^{18}F-FDG uptake tended to be higher than ^{18}F-BPA uptake. This may suggest that ^{18}F-BPA distribution in tumor tissue could be more specific for viable cancer cells compared with ^{18}F-FDG, whereas high ^{18}F-FDG uptake can be seen in activated macrophages and young granulation tissue as well as cancer cells [24].

The major limitations of the present study were the small patient population and limited histological variety. It should also be kept in mind that ^{18}F-FDG may not reflect ^{10}B concentrations or activity of amino acid transport systems. Even so, our findings suggest that the accumulation of ^{18}F-FDG may predict the accumulation of ^{18}F-BPA. Since ^{18}F-BPA synthesis is limited by low yield and high cost, it is not currently realistic to regularly use ^{18}F-BPA PET to screen all BNCT candidates, even in major hospitals. These constraints suggest that ^{18}F-FDG PET may have a role as an acceptable screening examination prior to ^{18}F-BPA PET for BNCT candidates with head and neck cancers. However, further research is called for, using a larger number of participants with selection of particular histological diagnostic criteria.

In conclusion, the accumulation of ^{18}F-FDG was correlated with that of ^{18}F-BPA in head and neck cancers. ^{18}F-FDG, which is the most popular tracer in PET studies and is available in many hospitals, may serve as an accessible way of predicting ^{18}F-BPA accumulation. ^{18}F-FDG PET might be an acceptable screening method prior to ^{18}F-BPA PET for BNCT candidates with head and neck cancers.

Grant support

This work was supported by the Cancer Research and Development Fund of the National Cancer Center (23-A-46), Japan.

Conflict of interest

All authors of this paper certify that there is no conflict of interest with any financial organization.

Acknowledgments

The authors thank Mr. Takayuki Nanma and the staff of SHI Accelerator Service Ltd. for their technical support. We thank Mr. Akira Hirayama and the staff of GE Healthcare for their technical support. We also thank Ms. Rieko Onoe for her secretarial support. Finally, we thank all the study participants and patients.

References

[1] Barth RF, Vicente MG, Harling OK, et al. Current status of boron neutron capture therapy of high grade gliomas and recurrent head and neck cancer. Radiat Oncol 2012;7:146–66.
[2] Henriksson R, Capala J, Michanek A, et al. Boron neutron capture therapy (BNCT) for glioblastoma multiforme: a phase II study evaluating a prolonged high-dose of boronophenylalanine (BPA). Radiother Oncol 2008;88:183–91.
[3] Menéndez PR, Roth BM, Pereira MD, et al. BNCT for skin melanoma in extremities: updated Argentine clinical results. Appl Radiat Isot 2009;67:50–3.
[4] Kankaanranta L, Saarilahti K, Mäkitie A, et al. Boron neutron capture therapy (BNCT) followed by intensity modulated chemoradiotherapy as primary treatment of large head and neck cancer with intracranial involvement. Radiother Oncol 2011;99:98–9.
[5] Herrera MS, González SJ, Minsky DM, et al. Evaluation of performance of an accelerator-based BNCT facility for the treatment of different tumor targets. Phys Med 2013;29:436–46.
[6] Ishiwata K, Ido T, Kawamura M, et al. 4-Borono-2-[18F]fluoro-D, L-phenylalanine as a target compound for boron neutron capture therapy: tumor imaging potential with positron emission tomography. Int J Rad Appl Instrum B 1991;18:745–51.
[7] Imahori Y, Ueda S, Ohmori Y, et al. Positron emission tomography-based boron neutron capture therapy using boronophenylalanine for high-grade gliomas: part I. Clin Cancer Res 1998;4:1825–32.
[8] Imahori Y, Ueda S, Ohmori Y, et al. Fluorine-18-labeled fluoroboronophenylalanine PET in patients with glioma. J Nucl Med 1998;39:325–33.
[9] Yoshimoto M, Kurihara H, Honda N, et al. Predominant contribution of L-type amino acid transporter to 4-borono-2-18F-fluoro-phenylalanine uptake in human glioblastoma cells. Nucl Med Biol 2013;40:625–9.
[10] Mochizuki T, Tsukamoto E, Kuge Y, et al. FDG uptake and glucose transporter subtype expressions in experimental tumor and inflammation models. J Nucl Med 2001;42:1551–5.
[11] Edet-Sanson A, Dubray B, Doyeux K, et al. Serial assessment of FDG-PET FDG uptake and functional volume during radiotherapy (RT) in patients with non-small cell lung cancer (NSCLC). Radiother Oncol 2012;1021:251–7.
[12] Wang LW, Wang SJ, Chu PY, et al. BNCT for locally recurrent head and neck cancer: preliminary clinical experience from a phase I/II trial at Tsing Hua Open-Pool Reactor. Appl Radiat Isot 2011;69:1803–6.
[13] Kankaanranta L, Seppälä T, Koivunoro H, et al. Boron neutron capture therapy in the treatment of locally recurred head-and-neck cancer: final analysis of a phase I/II trial. Int J Radiat Oncol Biol Phys 2012;82:e67–75.
[14] Suzuki M, Kato I, Aihara T, et al. Boron neutron capture therapy outcomes for advanced or recurrent head and neck cancer. J Radiat Res 2014;55:146–53.
[15] Ishiwata K, Ido T, Mejia AA, et al. Synthesis and radiation dosimetry of 4-borono-2-[18F]fluoro-D, L-phenylalanine a target compound for PET and boron neutron capture therapy. Int J Rad Appl Instrum A 1991;42:325–8.
[16] Miyashita M, Miyatake S, Imahori Y, et al. Evaluation of fluoridelabeled boronophenylalanine-PET imaging for the study of radiation effects in patients with glioblastomas. J Neurooncol 2008;89:239–46.
[17] Yanagida O, Kanai Y, Chairoungdua A, et al. Human L-type amino acid transporter 1 (LAT1): characterization of function and expression in tumor cell lines. Biochim Biophys Acta 2001;1514:291–302.
[18] Fuchs BC, Bode BP. Amino acid transporters ASCT2 and LAT1 in cancer: partners in crime? Semin Cancer Biol 2005;15:254–66.
[19] Haase C, Bergmann R, Fuechtner F, et al. L-type amino acid transporters LAT1 and LAT4 in cancer: uptake of 3-O-methyl-6-18 F-fluoro-Ldopa in human adenocarcinoma and squamous cell carcinoma in vitro and in vivo. J Nucl Med 2007;48:2063–71.
[20] Bodoy S, Martin L, Zorzano A, et al. Identification of LAT4, a novel amino acid transporter with system L activity. J Biol Chem 2005;280:12002–11.
[21] Sasaki M, Kuwabara Y, Ichiya Y, et al. Differential diagnosis of thymic tumors using a combination of 11C-Methionine PET and FDG PET. J Nucl Med 1999;40:1595–601.
[22] Kubota R, Kubota K, Yamada S, et al. Methionine uptake by tumor tissue: a microautoradiographic comparison with FDG. J Nucl Med 1995;36:484–92.
[23] Herholz K, Pietrzyk U, Vages J, et al. Correlation of glucose consumption and tumor cell density in astrocytoma. J Neurosurg 1993;79:853–8.
[24] Kubota K, Kubota R, Yamada S. FDG accumulation in tumor tissue. J Nucl Med 1993;34:419–21.

Eur Radiol (2014) 24:2532–2539
DOI 10.1007/s00330-014-3233-7

MAGNETIC RESONANCE

Does Gadoxetic acid-enhanced 3.0T MRI in addition to 64-detector-row contrast-enhanced CT provide better diagnostic performance and change the therapeutic strategy for the preoperative evaluation of colorectal liver metastases?

Keitaro Sofue · Masakatsu Tsurusaki · Takamichi Murakami · Shunsuke Onoe · Hiroyuki Tokue · Kentaro Shibamoto · Yasuaki Arai · Kazuro Sugimura

Received: 11 January 2014 / Revised: 28 April 2014 / Accepted: 9 May 2014 / Published online: 28 May 2014

Abstract
Objectives To compare diagnostic performance in the detection of colorectal liver metastases between 64-detector-row contrast-enhanced CT (CE-CT) alone and the combination of CE-CT and gadoxetic acid-enhanced MRI (EOB-MRI) at 3.0T, and to assess whether EOB-MRI in addition to CE-CT results in a change to initially planned operative strategy.
Methods A total of 39 patients (27 men, mean age 65 years) with 85 histopathologically confirmed liver metastases were included. At EOB-MRI, unenhanced (T1- and T2-weighted), dynamic, and hepatocyte-phase images were obtained. At CE-CT, four-phase dynamic contrast-enhanced images were obtained. One on-site reader and three off-site readers independently reviewed both CE-CT alone and the combination of CE-CT and EOB-MRI. Sensitivity, positive predictive value, and alternative free-response receiver operating characteristic (AFROC) method were calculated. Differences in therapeutic strategy before and after the EOB-MRI examination were also evaluated.
Results Sensitivity and area under the AFROC curve with the combination of CE-CT and EOB-MRI were significantly superior to those with CE-CT alone. Changes in surgical therapy were documented in 13 of 39 patients.
Conclusions The combination of CE-CT and EOB-MRI may provide better diagnostic performance than CE-CT alone for the detection of colorectal liver metastases, and EOB-MRI in addition to CE-CT resulted in changes to the planned operative strategy in one-third of the patients.

Key Points
- *Accurate preoperative imaging is essential for surgical planning and successful hepatic resection.*
- *Combination of CE-CT and EOB-MRI is useful to detect colorectal liver metastases.*
- *EOB-MRI combined with CE-CT contributes to determine the correct therapeutic strategy.*

Keywords Colorectal liver metastases · Gadoxetic acid-enhanced magnetic resonance imaging · Contrast-enhanced computed tomography · Diagnostic performance · Therapeutic strategy

K. Sofue · M. Tsurusaki · H. Tokue · K. Shibamoto · Y. Arai
Division of Diagnostic Radiology, National Cancer Center Hospital, Tokyo, Japan

K. Sofue · K. Sugimura
Department of Radiology, Graduate School of Medicine, Kobe University, Kobe, Japan

M. Tsurusaki (✉) · T. Murakami
Department of Radiology, Faculty of Medicine, Kinki University, 377-2 Ohnohigashi, Osakasayama, Osaka 589-8511, Japan
e-mail: mtsuru@dk2.so-net.ne.jp

S. Onoe
Department of Hepatobiliary and Pancreatic Surgery, National Cancer Center Hospital, Tokyo, Japan

Introduction

Metastasis to the liver is the most common site of haematogenous spread in patients with colorectal cancer, with 40 % of stage IV patients having only liver metastatic disease [1]. Hepatic resection has emerged as a promising treatment option to improve long-term survival, and resectability criteria include complete resection of metastatic lesions while preserving future liver remnants as much as possible [2, 3]. Therefore, accurate assessment with preoperative imaging,

including the number, size, and location of the lesions as well as the number of involved liver segments, is essential for adequate surgical planning and successful hepatic resection [2, 3].

Multidetector computed tomography (MDCT), using intravenous contrast agents, is routinely employed for the staging of follow-up of patients, and it provides robust and rapid imaging of the chest, abdomen, and pelvis for the detection of liver and extrahepatic metastases. In addition, major advances in liver magnetic resonance imaging (MRI) include the development of high-resolution volumetric imaging approaching the resolution of MDCT, parallel imaging to reduce imaging time, and higher magnetic field strength using a 3.0T system [4].

Gadoxetic acid is a liver-specific MR contrast agent that offers dynamic and static hepatocyte imaging to improve the detection and characterization of focal liver lesions [5], including liver metastases [6–8]. Some studies have compared gadoxetic acid-enhanced MRI (EOB-MRI) and contrast-enhanced MDCT [9, 10], although only two studies have compared EOB-MRI at 3.0T with contrast-enhanced 64-row MDCT for the detection of colorectal liver metastases [11, 12]. And while EOB-MRI has been clinically performed after CT examination for preoperative imaging of colorectal liver metastases, no studies have assessed the diagnostic performance of EOB-MRI combined with contrast-enhanced MDCT to determine the best therapeutic strategy.

The present study compared the diagnostic performance of the 64-detector-row CE-CT alone and in combination with EOB-MRI at 3.0T for the detection of colorectal liver metastases, and assessed whether the combination findings resulted in a change to the initially planned operative strategy.

Materials and methods

Patient populations

Forty-seven consecutive patients suspected of having liver metastases on the basis of their history of colorectal cancer and previous ultrasound findings and/or elevation of carcinoembryonic antigen (CEA) were examined by CE-CT followed by EOB-MRI at our institution in order to acquire additional information prior to surgical liver resection. EOB-MRI was performed within four weeks prior to surgery, and the interval between the CE-CT and EOB-MRI was two weeks or less. All patients had previously undergone surgery at the primary site and had histopathological confirmation of colorectal cancer. Eight of the 47 patients were excluded from our study because they had received previous chemotherapy for liver metastases. The remaining 39 patients (27 men and 12 women) were included. The mean age of the patients was 65 years (range, 45–79 years).

Thirty-seven of these 39 patients had a total of 85 liver metastases, which were diagnosed by histopathological examination of surgical specimens and intraoperative ultrasound (US) in 34 patients and on the basis of tumour growth observed during follow-up examinations in three patients who were not candidates for liver resection. In the remaining two patients, it was confirmed that liver metastases were not evident from imaging examinations and CEA levels during ≥6 months of follow-up. The institutional review board of our institution approved the study, and informed consent was obtained from each patient before enrolment. This study was conducted in accordance with the amended Helsinki Declaration.

CT imaging protocol

CT images were obtained using 64-detector-row MDCT instruments (Aquilion 64; Toshiba Medical System, Tokyo, Japan) with a 0.4-s rotation time and exposure factors of 120 kV and 160 mAs for all images. A total of 100 ml of the contrast material (Iopamiron 300/370; Bayer Schering Pharma, Osaka, Japan) was injected into an antecubital vein at a rate of 3.3 ml/s using an automatic power injector (Mark V ProVis; Medrad, Indianola, PA). An iodine concentration of 300 mg I/ml (Iopamiron 300) was used when the patient's body weight was <50 kg, and 370 mg I/ml (Iopamiron 370) was used when body weight was >50 kg. The examinations were performed in a cephalocaudal direction, starting at the top of the liver, and each examination included non-enhanced and contrast-enhanced imaging.

After non-enhanced imaging was performed in the transverse section, CE-CT was performed for 35 s (arterial phase), 70 s (portal phase), and 120 s (equilibrium phase), after intravenous administration of the contrast material. The following imaging parameters were used: collimation of 32× 1 mm, pitch factor of 0.656, rotation time of 0.5 s, and 5-mm reconstruction interval (slice thickness). A standard algorithm was used for all image displays.

MR imaging protocol

A superconducting magnet system in a 3.0T (Magnetom Trio; Siemens Medical Solutions, Erlangen, Germany) using an eight-channel body phased-array coil was used to perform EOB-MRI. A 45 mT/m gradient field strength and slew rate of 200T/m/s were used to actively shield the magnet. After breath-hold, double-echo T1-weighted gradient-echo (GRE) images (in-phase and opposed-phase images) and navigator-triggered fat-suppressed T2-weighted turbo spin-echo (TSE) images using prospective acquisition correction (PACE) were obtained, and dynamic images using fat-suppressed T1-weighted GRE images with a three-dimensional volumetric interpolated breath-hold examination (3D-VIBE) sequence

were obtained before (pre-contrast) and 14–30 s (arterial phase), 70 s, and 3 min after intravenous administration of gadoxetic acid (Primovist; Bayer Schering Pharma, Osaka, Japan), which was injected as a bolus (2.0 ml/s) at a dose of 0.025 mmol/kg of body weight, followed by 20 ml of a saline flush. Hepatocyte-phase images were obtained 20 min after the injection of gadoxetic acid.

The following parameters were used to acquire breath-hold T1-weighted GRE images: repetition time (TR), 120 ms; echo time (TE), 2.46 m; flip angle, 66°; matrix, 320×180; number of signals acquired, one; section thickness, 7 mm; intersectional gap, 1.4 mm; and acquisition time, 28 s. PACE using the following parameters was used to acquire navigator-triggered fat-suppressed T2-weighted TSE images: TR (effective), 3865–5534 ms; TE (effective), 71 ms; flip angle, 120°; echo train length, 12; matrix, 384×202; number of signals acquired, one; section thickness, 7 mm; intersectional gap, 1.4 mm; and acquisition time, approximately 90 s. A 3D-VIBE sequence with the following parameters was used to acquire fat-suppressed T1-weighted GRE images: TR, 3.68; TE, 1.22; flip angle, 10°; matrix, 256×192; number of signals acquired, one; section thickness, 3 mm; intersectional gap, 0.6 mm; and acquisition time, 21 s.

Standard of reference

In this study, a single radiologist (12 years of experience as a radiologist) and a single surgeon (13 years of experience as a surgeon) determined the presence or absence of liver metastases on the basis of findings obtained at definitive surgery that involved intraoperative US or an increase in size on the imaging examinations over a six-month follow-up period. Hepatic resection and intraoperative US for the non-resected segments were performed by surgeons who were aware of the preoperative MRI findings. The resected specimens at 5-mm intervals in the transverse plane were sectioned by a single pathologist, and the radiologist and pathologist compared the findings with those of EOB-MRI.

Liver metastases were measured on resected specimens and EOB-MRI, and their mean tumour size along the long axis was 2.5 cm (range, 0.5–14.0 cm). Twenty-six of the 85 lesions were <10 mm in diameter (mean, 0.68 mm; range, 0.4–1.0 cm). Seventeen patients had 42 benign hepatic lesions. Of these, 15 patients had a total of 30 cysts (mean size, 1.7 cm; range, 0.8–4.7 cm). Five of these 17 patients had a total of 12 haemangiomas (mean size, 0.9 cm; range, 0.8–2.8 cm). The cysts and haemangiomas were diagnosed on the basis of typical radiological examination findings and by the fact that the lesions demonstrated no change in size on the follow-up examinations performed over a period of ≥12 months (range, 12–31 months).

Image analysis

Image evaluation was performed as an on-site assessment by one clinical investigator (12 years of experience as a radiologist at the institution) and separately as blinded reading by three investigators (19, 13, and 11 years of experience as radiologists) who were not involved in the clinical investigation (off-site readers). In the on-site evaluation, the reader was not blinded to any imaging, pathological or laboratory results relevant to the patient's care. Meanwhile, three off-site readers were aware of the overall goal of the study before the reading session but were unaware of any other information.

Image evaluation in the clinical part of the study (on-site assessment) included a separate assessment of CE-CT images and the combination of CE-CT and EOB-MR images. Image evaluation in the blinded reading of each patient (off-site assessment) was performed in random order. Each reader independently interpreted the CE-CT images, and the readers then viewed EOB-MRI for the patient and re-evaluated and recorded their findings on the combination of CE-CT and EOB-MRI in a similar manner.

In the on-site and off-site evaluations, the readers recorded the presence, location, and size of all focal liver lesions at the segment on schematic drawings of transverse sections of the whole liver to avoid confusion in data analysis. Following this, they assigned a confidence level to each lesion on a four-point scale: 1, probably not liver metastasis; 2, possibly liver metastasis; 3, probably liver metastasis; and 4, definitely liver metastasis. All images were reviewed on a 1536×2048 picture archiving and communication system (PACS) monitor (RadICS, Nihon IBM, Tokyo, Japan).

The criteria for the radiological diagnoses of liver metastasis on CE-CT were described as an ill-defined heterogeneous nodule with higher attenuation than that of bile with some degree of enhancement. The criteria for liver metastasis on EOB-MRI were focal discrete nodular lesions showing high signal intensity relative to the liver parenchyma on T2-weighted FSE images (and lower signal intensity than the gallbladder or cerebrospinal fluid) and low signal intensity relative to the liver parenchyma on T1-weighted GRE images obtained at 70 s and 3 min after gadoxetic acid injection, and more conspicuous on the hepatocyte-phase images. The diagnosis of liver metastases was more definitive when perilesional enhancement was detected on the T1-weighted GRE images obtained 30 s after gadoxetic acid injection.

Change in therapeutic strategy

In the on-site evaluation, the indications for surgical therapy and the planned surgical procedure were provided at two different time points by the clinical radiologist and a surgeon, before and after EOB-MRI examination. The potential planned surgical procedures were hemihepatectomy,

segmentectomy, atypical segmentectomy, and metastasectomy. In addition, watchful waiting was adopted when no liver metastases were evident, and chemotherapy or conservative therapy was performed when surgical intervention was impossible. The planned therapies before and after EOB-MRI examination were compared with the surgical procedure ultimately performed.

Statistical analysis

The sensitivities and positive predictive values (PPVs) of CE-CT alone and the combination of CE-CT and EOB-MRI for the detection of liver metastases were calculated in the on-site evaluation by one reader, and were assessed in the off-site evaluation by each reader using the number of lesions assigned a confidence score of 3 or 4 (i.e., probably liver metastasis or definitely liver metastasis) from the total number of liver metastases. McNemar's test and Fisher's exact test were utilized to compare the sensitivities and PPVs for CE-CT alone and the combination of CE-CT and EOB-MRI among the composite data.

A maximum-likelihood estimation program (ROCKIT 0.9B; C.E. Metz, University of Chicago, Chicago, Ill, 1998) was used to calculate the alternative free-response receiver operating characteristic (AFROC) curve for each reader and each image set in the off-site evaluation. The area under each AFROC curve (Az) indicated the overall diagnostic accuracy of each image set and each reader. A univariate z score test was utilized to test differences between the mean Az values for statistical significance.

Interobserver variability in the off-site evaluation was assessed by calculating the κ statistic for multiple observers using non-weighted κ statistics with binary data defined by the presence or absence of liver metastases. κ values of 0.01–0.20 were considered to indicate poor agreement; 0.21–0.40, fair agreement; 0.41–0.60, moderate agreement; 0.61–0.80, good agreement; and 0.81–1.0, excellent agreement.

For all tests, a p value <0.05 was considered to indicate statistical significance. A software package (SPSS 12.0 for Windows, SPSS (IBM), Chicago, IL) was used to perform statistical analyses.

Results

Image analysis of on-site data

At the on-site evaluation, the detection sensitivity of liver metastases with the combination of CE-CT and EOB-MRI was significantly higher than that of CE-CT alone, and there was no significant difference in PPVs between CE-CT alone and the combination of CE-CT and EOB-MRI (Table 1).

Table 1 Sensitivity and positive predictive value for the detection of liver metastases on contrast-enhanced CT and gadoxetic acid-enhanced MR imaging by on-site readers

	CECT alone	CECT and EOB-MRI	p value
Mean	Sensitivity (%)		
	78.8 (67/85)	92.9 (79/85)	0.006
Mean	Positive Predictive Value (%)		
	91.8 (67/73)	94.0 (79/84)	0.408

Note: Data in parentheses are numbers used to calculate sensitivity and positive predictive value.

CECT contrast-enhanced CT

EOB-MRI gadoxetic acid-enhanced enhanced MR images

Image analysis of off-site data

In the off-site evaluation, the detection sensitivity of the combination of CE-CT and EOB-MRI was significantly higher than that of the CE-CT alone for each of the three readers (Table 2). No significant differences were found in PPVs between CE-CT alone and the combination of CE-CT and EOB-MRI for any of the three observers.

For the three readers, 16 false-positive lesions were recorded on CE-CT alone and 10 were recorded on the combination of CE-CT and EOB-MRI. On CE-CT alone, six cysts and four haemangiomas were diagnosed as liver metastases (all <1.0 cm), three false-positive findings were attributed to thrombosed vessels (one, 1.2 cm; two, <1.0 cm), two were attributed to partial volume averaging (<1.0 cm), and the remaining one was unexplained. On the combination of CE-CT and EOB-MRI, two cysts and two haemangiomas were misdiagnosed as metastases (all <1.0 cm), four false-positive findings were attributed to intrahepatic vasculature (one, <1.5 cm; five, <1.0 cm), and the remaining two were unexplained sub-centimetre areas on the hepatocyte-phase images.

With regard to the false-negative lesions, none of the readers detected five lesions in three patients on either CE-CT alone or the combination of CE-CT and MRI (all were ≤1.0 cm). Two of these five lesions were detected by intraoperative US, one was detected by surgical palpation, and one was detected only by histopathological inspection. Using CE-CT alone, 11 lesions in eight patients were not detected with a high confidence level by any of the readers. On the other hand, six of these lesions in five patients were detected by at least one reader using the combination of CE-CT and EOB-MRI (Fig. 1).

Statistically significant differences in the Az values for CE-CT alone and the combination of CE-CT and EOB-MRI were demonstrated in the off-site evaluation by each of the three readers (mean Az values for Gd-EOB-DTPA-enhanced MR images, 0.948; mean Az values for CE-CT, 0.859; p=0.034) (Table 3).

Table 2 Sensitivity and positive predictive value for the detection of liver metastases on contrast-enhanced CT and gadoxetic acid-enhanced MR imaging by off-site readers

	CECT alone	CECT and EOB-MRI	*p* value
	Sensitivity (%)		
Reader 1	77.6 (66/85)	91.8 (78/85)	0.008
Reader 2	76.5 (65/85)	87.1 (74/85)	0.014
Reader 3	83.5 (71/85)	94.1 (80/85)	0.035
Mean	79.2 (202/255)	91.0 (232/255)	0.026
	Positive Predictive Value (%)		
Reader 1	90.4 (66/73)	95.1 (78/82)	0.108
Reader 2	92.9 (65/70)	96.1 (74/77)	0.626
Reader 3	94.7 (71/75)	96.3 (80/83)	0.288
Mean	92.7 (202/218)	95.8 (232/242)	0.423

Note: Data in parentheses are numbers used to calculate sensitivity and positive predictive value.

CECT contrast-enhanced CT

EOB-MRI gadoxetic acid-enhanced enhanced MR images

The κ values for the three readers were 0.62 for CE-CT alone and 0.70 for the combination of CE-CT and EOB-MRI. These results indicated good interobserver agreement with regard to the presence of liver metastases.

Table 3 Az values for the detection of hepatic metastases on contrast-enhanced CT and Gd-EOB-DTPA enhanced MR imaging by off-site readers

	CECT alone	CECT and EOB-MRI	*P* value*
Reader 1	0.843	0.916	0.03
Reader 2	0.832	0.902	0.042
Reader 3	0.879	0.948	0.024
Mean	0.853	0.929	0.034

CECT contrast-enhanced CT

EOB-MRI gadoxetic acid-enhanced enhanced MR images

Change in therapeutic strategy of on-site data (Fig. 2)

The following surgical procedures were performed: right lobectomy in two patients, right lobectomy and metastatectomy in three, right anterior segmentectomy in five, right anterior segmentectomy and metastatectomy in two, right posterior segmentectomy in three, right posterior segmentectomy and metastatectomy in one, left lobectomy in one, left lobectomy and metastatectomy in three, left lateral segmentectomy in four, and left lateral segmentectomy and metastatectomy in one patient.

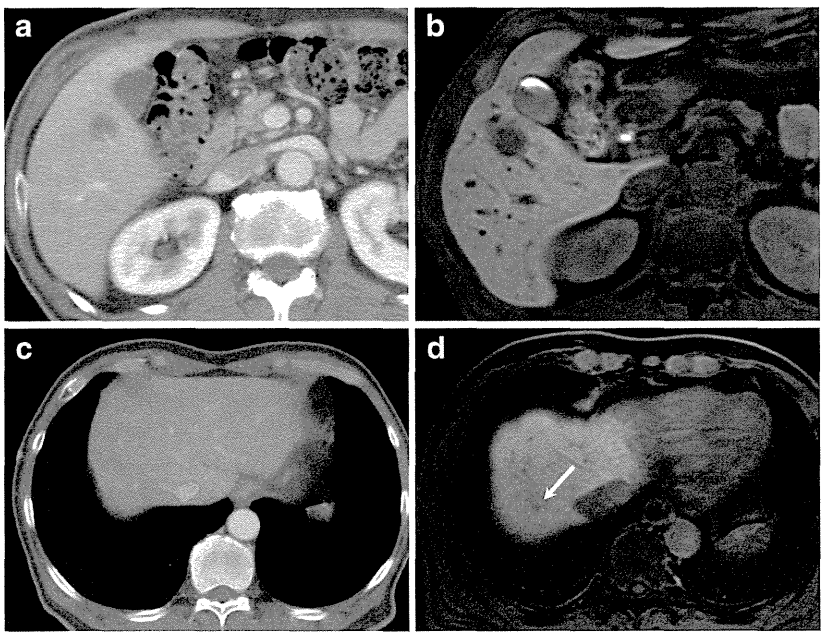

Fig. 1 Surgically-proved liver metastases from colon cancer in a 67-year-old man. A 16 mm diameter liver metastasis could be detected in segment 5 on both portal phase of CE-CT images (**a**) and hepatocyte-phase of gadoxetic acid-enhanced T1-weighted GRE images (**b**). On hepatocyte-phase (**d**) of gadoxetic acid-enhanced T1-weighted GRE images, additional sub-centimetre metastasis was identified in segment 7 (white arrow), although the lesion was not detected on portal phase of CE-CT images (**c**). Before the EOB-MRI examination, the planned surgical procedure was right anterior partial segmentectomy. After the EOB-MRI examination, the planned therapeutic strategy was changed to right anterior partial segmentectomy and metastatectomy

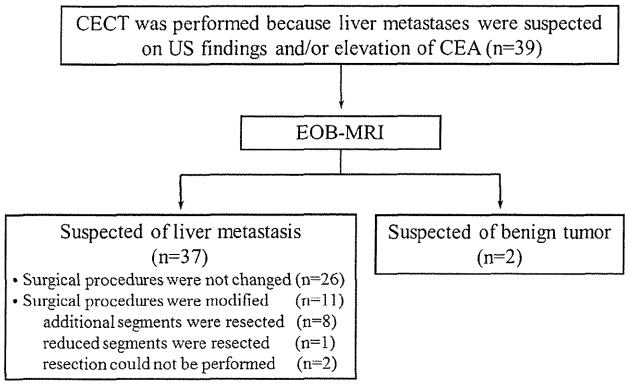

Fig. 2 Flow diagram shows changing diagnosis and therapy of a patient who was suspected of having liver metastasis from colorectal cancer, and underwent both CE-CT and EOB-MRI

In 13 of the 39 patients (33.3 %), the planned therapeutic strategy was changed after EOB-MRI examination at the on-site assessment. In 11 of these 13 patients, planned surgical procedures were ultimately modified on the basis of the combination of CE-CT and EOB-MRI findings. Additional segmentectomy or metastatectomy was performed in eight patients; additional lesions excluding the possibility of resection were detected and reduced segments were resected in one patient; and no surgical resection was performed due to multiple liver metastases in bilateral liver lobes and peritoneal dissemination at surgery in one each. In the remaining two of these 13 patients, each suspected liver metastasis on CE-CT was confirmed as a liver cyst by EOB-MRI findings. Watchful waiting was adopted for these patients, and the lesions demonstrated no change in size at follow-up examinations 15 and 18 months later.

In 26 of the 39 patients, the planned therapeutic strategy prior to EOB-MRI was unchanged after EOB-MRI. Of these 26 patients, although two had an additional lesion on EOB-MRI, a change in therapeutic strategy was unnecessary because the location of the missed lesions on CE-CT did not result in alteration of the surgical procedure.

Discussion

The results of this study demonstrate that the combination of CE-CT and EOB-MRI showed significantly higher detection of liver metastases than CE-CT alone. Moreover, the planned therapeutic strategy was changed in one-third of the patients after EOB-MRI examination. These findings indicate that, with the use of state-of-the-art 64-row MDCT and 3.0T MR system, EOB-MRI can provide information in addition to that provided by CE-CT for preoperative evaluation of colorectal liver metastases, frequently resulting in a change in therapeutic strategy.

Our results revealed that, for all readers, the combined reading of CE-CT and EOB-MRI yielded significantly higher detection sensitivity and resulted in better diagnostic performance for liver metastases than CE-CT alone. Moreover, the detection sensitivity of the combination of CE-CT and EOB-MRI for liver metastases in the present study was higher than that reported in several previous studies that used 1.0T–1.5T MRI [8]. The higher detection sensitivity in this study can be explained by the fact that 3.0T MRI provides a higher signal-to-noise ratio (SNR), and the increased SNR and contrast-to-noise ratio on hepatocyte-phase 3D-GRE images allowed us to obtain higher spatial resolution, such as thinner-slice images, than can be obtained at a lower field strength, resulting in improvement of the conspicuity and detectability of liver metastases [13, 14]. However, a potential drawback of EOB-MRI is the lack of an equilibrium phase in the real sense of the term, which makes it difficult to distinguish liver metastases from haemangiomas, particularly in sub-centimetre lesions that do not show peripheral globular enhancement on arterial-phase images [15, 16]. The shortcomings of EOB-MRI can be overcome by multiphase CE-CT [16], which also supports our result that PPV with the combination of CE-CT and EOB-MRI in this study was superior to that of EOB-MRI in previous reports [11–13]. However, in contrast to the findings of previous studies (Table 4), we did not clearly demonstrate the superiority of EOB-MRI at 3.0T over 1.5T or the superiority of the combination of CE-CT and EOB-MRI over EOB-MRI alone. Further studies are needed to elucidate the superiority of 3.0T EOB-MRI or the combination of CE-CT and EOB-MRI for the detection of colorectal liver metastases as compared to 1.5T EOB-MRI or EOB-MRI alone.

In our study, the planned therapeutic strategy was changed in 13 of the 39 patients (33.3 %) on the basis of the EOB-MRI examination findings, a rate that is higher than that in a previous report [8]. This discrepancy may be due to the fact that some patients in the previous study had hepatocellular carcinoma with chronic liver disease, which may have caused less hepatocyte uptake of gadoxetic acid than in the case of a non-cirrhotic liver, resulting in a lower tumour-to-liver contrast [17]. Another possible explanation is that Hammerstingl et al. [8] used 1.0T–1.5T MRI, whereas we used 3.0T MRI, and MRI with a 3.0T field provided a higher contrast-to-noise ratio than lower-field-strength MRI [14]. Furthermore, the combination of CE-CT and EOB-MRI could minimize residual liver metastases by detecting the number of lesions more precisely, and could avoid redundant surgery by differentiating liver metastases from benign lesions. These findings indicate that EOB-MRI, with a state-of-the-art 64-detector-row CE-CT and 3.0T MR system, can provide information beyond that of CE-CT for preoperative evaluation of colorectal liver metastases and can improve the accuracy of the therapeutic strategy, including preoperative planning of liver resection.

Table 4 Comparison with previous articles on CE-CE and EOB-MRI for the detection of colorectal liver metastases

Article	CT and MRI unit	CE-CT			EOB-MRI		
		Sensitivity	Specificity	PPV	Sensitivity	Specificity	PPV
Hammerstingl R, et al. [8]	CT; unknown MRI; 1.0–1.5T	77.1 %	88.5 %	None	87.4 %	90.1 %	None
Muhi A, et al. [9]	CT; 16-detector row MRI; 1.5T	63 %	None	96 %	95 %	None	98 %
Kim YK, et al. [10]	CT; 16-detector row MRI; 1.5T	75 %	96 %	None	96 %	98 %	None
Scharitzer M, et al. [11]	CT; 64-detector row MRI; 3.0T	82.8 %	96.5 %	None	91.2 %	97.1 %	None
Berger-Kulemann V, et al. [12]	CT; 64-detector row MRI; 3.0T	72.1 %	None	None	97.1 %	None	None
Sofue K, et al. [13]	CT; not examined MRI; 3.0T	None	None	None	92.0 %	None	94.2 %
Present study	CT; 64-detector row MRI; 3.0T	79.2 %	None	92.7 %	91.0 %	None	95.8 %

Note: None indicates that data were not expressed in the paper.

CECT contrast-enhanced CT

EOB-MRI gadoxetic acid-enhanced enhanced MR images

This study had several limitations. First, it was conducted in a highly selected population of patients with colorectal cancer scheduled for surgery, which resulted in a higher level of suspicion on image analysis among the readers. However, image evaluation was performed by on-site and off-site blinded readers who were unaware of any information regarding tumour burden. Second, the findings of true-positive lesions were not completely accurate, as the exact number of liver metastases in non-resected liver segments could not be determined and specificity could not be calculated. However, we performed intensive evaluation of the non-resected liver segments by intraoperative US, and follow-up examinations were available for all lesions in the non-resected segments to minimize the number of false-negative lesions. Third, diffusion-weighted imaging (DWI) pulse sequences and positron emission tomography (PET) were not used in the analyses. DWI and PET may have additional value for the detection of liver metastases and differentiation from cysts and haemangiomas [18–20]. DWI and PET in addition to EOB-MRI may lead to improvement in diagnostic performance for detecting small liver metastases. Fourth, the number of sub-centimetre liver metastases was small. Further studies in a larger series should be performed to evaluate the detectability of tiny liver metastases. Finally, only liver metastases were assessed in image analysis, and extrahepatic metastases were not evaluated and compared between CE-CT and EOB-MRI. Extrahepatic metastases preclude surgical resection of liver metastases and affect the prognosis and survival of patients [20]. Further validation studies are needed to clarify the role of EOB-MRI for the detection of metastases in patients with colorectal cancer.

In conclusion, our study showed that the combination of CE-CT and EOB-MRI provided significantly higher sensitivity, and thus better diagnostic performance, than CE-CT alone for the detection of colorectal liver metastases in a preoperative setting. Indeed, the initially planned surgery was altered in one-third of the patients after EOB-MRI examination. EOB-MRI combined with CE-CT contributed to improved determination of appropriate therapeutic strategies, which may lead to better prognosis and survival of patients.

Acknowledgments The scientific guarantor of this publication is Masakatsu Tsurusaki. The authors of this manuscript declare no relationships with any companies, whose products or services may be related to the subject matter of the article. The authors state that this work has not received any funding. One of the authors has significant statistical expertise. Institutional Review Board approval was obtained. Written informed consent was obtained from all subjects (patients) in this study. Methodology: prospective, diagnostic or prognostic study, performed at one institution.

References

1. Manfredi S, Lepage C, Hatem C, Coatmeur O, Faivre J, Bouvier AM (2006) Epidemiology and management of liver metastases from colorectal cancer. Ann Surg 244:254–259
2. Charnsangavej C, Clary B, Fong Y, Grothey A, Pawlik TM, Choti MA (2006) Selection of patients for resection of hepatic colorectal metastases: expert consensus statement. Ann Surg Oncol 13:1261–1268
3. Frankel TL, Gian RK, Jarnagin WR (2012) Preoperative imaging for hepatic resection of colorectal cancer metastasis. J Gastrointest Oncol 3:11–18
4. von Falkenhausen MM, Lutterbey G, Morakkabati-Spitz N, Walter O, Gieseke J, Blömer R et al (2006) High-field-strength MR imaging

of the liver at 3.0 T: intraindividual comparative study with MR imaging at 1.5 T. Radiology 241:156–166
5. Huppertz A, Haraida S, Kraus A, Zech CJ, Scheidler J, Breuer J et al (2005) Enhancement of focal liver lesions at gadoxetic acid-enhanced MR imaging: correlation with histopathologic findings and spiral CT—initial observations. Radiology 234:468–478
6. Ward J (2006) New MR techniques for the detection of liver metastases. Cancer Imaging 6:33–42
7. Zech CJ, Herrmann KA, Reiser MF, Schoenberg SO (2007) MR imaging in patients with suspected liver metastases: value of liver-specific contrast agent Gd-EOB-DTPA. Magn Reson Med Sci 6:43–52
8. Hammerstingl R, Huppertz A, Breuer J, Balzer T, Blakeborough A, Carter R et al (2008) Diagnostic efficacy of gadoxetic acid (Primovist)-enhanced MRI and spiral CT for a therapeutic strategy: comparison with intraoperative and histopathologic findings in focal liver lesions. Eur Radiol 18:457–467
9. Muhi A, Ichikawa T, Motosugi U, Sou H, Nakajima H, Sano K et al (2011) Diagnosis of colorectal hepatic metastases: comparison of contrast-enhanced CT, contrast-enhanced US, superparamagnetic iron oxide-enhanced MRI, and gadoxetic acid-enhanced MRI. J Magn Reson Imaging 34:326–335
10. Kim YK, Park G, Kim CS, Yu HC, Han YM (2012) Diagnostic efficacy of gadoxetic acid-enhanced MRI for the detection and characterization of liver metastases: comparison with multidetector-row CT. Br J Radiol 85:539–547
11. Scharitzer M, Ba-Ssalamah A, Ringl H, Kölblinger C, Grünberger T, Weber M et al (2013) Preoperative evaluation of colorectal liver metastases: comparison between gadoxetic acid-enhanced 3.0-T MRI and contrast-enhanced MDCT with histopathological correlation. Eur Radiol 23:2187–2196
12. Berger-Kulemann V, Schima W, Baroud S, Koelblinger C, Kaczirek K, Gruenberger T et al (2012) Gadoxetic acid-enhanced 3.0 T MR imaging versus multidetector-row CT in the detection of colorectal metastases in fatty liver using intraoperative ultrasound and histopathology as a standard of reference. Eur J Surg Oncol 38:670–676
13. Sofue K, Tsurusaki M, Tokue H, Arai Y, Sugimura K (2011) Gd-EOB-DTPA-enhanced 3.0 T MR imaging: quantitative and qualitative comparison of hepatocyte-phase images obtained 10 min and 20 min after injection for the detection of liver metastases from colorectal carcinoma. Eur Radiol 21:2336–2343
14. Chang KJ, Kamel IR, Macura KJ, Bluemke DA (2008) 3.0-T MR imaging of the abdomen: comparison with 1.5 T. Radiographics 28: 1983–1998
15. Goshima S, Kanematsu M, Watanabe H, Kondo H, Shiratori Y, Onozuka M et al (2010) Hepatic hemangioma and metastasis: differentiation with gadoxetate disodium-enhanced 3-T MRI. AJR Am J Roentgenol 195:941–946
16. Tateyama A, Fukukura Y, Takumi K, Shindo T, Kumagae Y, Kamimura K et al (2012) Gd-EOB-DTPA-enhanced magnetic resonance imaging features of hepatic hemangioma compared with enhanced computed tomography. World J Gastroenterol 18:6269–6276
17. Motosugi U, Ichikawa T, Sou H, Sano K, Tominaga L, Kitamura T et al (2009) Liver parenchymal enhancement of hepatocyte-phase images in Gd-EOB-DTPA-enhanced MR imaging: which biological markers of the liver function affect the enhancement? J Magn Reson Imaging 30:1042–1046
18. Kim YK, Lee MW, Lee WJ, Kim SH, Rhim H, Lim JH et al (2012) Diagnostic accuracy and sensitivity of diffusion-weighted and of gadoxetic acid-enhanced 3-T MR imaging alone or in combination in the detection of small liver metastasis (≤1.5 cm in diameter). Investig Radiol 47:159–166
19. Donati OF, Fischer MA, Chuck N, Hunziker R, Weishaupt D, Reiner CS (2013) Accuracy and confidence of Gd-EOB-DTPA enhanced MRI and diffusion-weighted imaging alone and in combination for the diagnosis of liver metastases. Eur J Radiol 82:822–828
20. Seo HJ, Kim MJ, Lee JD, Chung WS, Kim YE (2011) Gadoxetate disodium-enhanced magnetic resonance imaging versus contrast-enhanced 18F-fluorodeoxyglucose positron emission tomography/computed tomography for the detection of colorectal liver metastases. Investig Radiol 46:548–555

Surg Today (2014) 44:2366–2368
DOI 10.1007/s00595-013-0745-8

CASE REPORT

Infusion of 50 % glucose solution to occlude an intrahepatic portosystemic venous shunt before percutaneous transhepatic portal embolization: report of a case

Keitaro Sofue · Yoshito Takeuchi · Kentaro Shibamoto · Koji Sugimoto · Kazuro Sugimura · Yasuaki Arai

Received: 25 January 2013 / Accepted: 18 July 2013 / Published online: 4 October 2013

Abstract A 68-year-old man with cholangiocarcinoma underwent percutaneous transhepatic portal embolization to expand the indication for hepatic resection. Selective right posterior portography revealed an intrahepatic portosystemic venous shunt (IPSVS) connecting the segment VII branch to the right hepatic venous branch. An infusion of 50 % glucose solution was given to occlude the shunt. This is novel management for IPSVSs when they are numerous, small, or torturous, and makes the subsequent procedures simpler, shorter, and less expensive.

Keywords Percutaneous transhepatic portal embolization · Intrahepatic portovenous shunt · Glucose solution

Introduction

Percutaneous transhepatic portal embolization (PTPE) is performed to expand the indications for major hepatic resection. Various embolic agents are used to achieve this and include gelatin sponge, fibrin glue, polyvinyl alcohol particles, cyanoacrylate and ethiodized oil, and absolute ethanol [1, 2].

Intrahepatic portosystemic venous shunts (IPSVS) can be congenital or may develop secondary to portal hypertension or trauma [3, 4]. For patients with an IPSVS, the therapeutic effect of PTPE is insufficient because of overflow of the embolic agent into the systemic circulation, potentially resulting in non-targeted embolization of the pulmonary artery. In this situation, blood flow through the portosystemic shunt must be stopped. An IPSVS is usually embolized with microcoils or particles [3, 5]; however, this can be difficult when there are numerous shunts or the shunt is small or torturous.

We report a case of PTPE coexisting with an IPSVS which was successfully occluded with an infusion of 50 % glucose solution.

Case report

A 68-year-old man with cholangiocarcinoma underwent preoperative PVE to induce selective hypertrophy and expand the indication for extended right hepatic resection. Contrast-enhanced computed tomography of the abdomen did not reveal an anomalous portovenous shunt. The right anterior branch of portal vein was punctured percutaneously with a 21-gauze needle (Top, Tokyo, Japan) under ultrasonographic guidance. A 5-French (F) sheath (Introducer set; Medikit, Tokyo, Japan) was advanced into the portal vein using the Seldinger technique under fluoroscopic guidance. A reverse-curved 5-F balloon catheter with a tip hole (Selecon balloon catheter; Terumo-Clinical Supply, Gifu, Japan) was also inserted into the posterior branch of the portal vein.

Selective right posterior portography was done with balloon occlusion, revealing an IPSVS connecting the segment VII branch to the right hepatic venous branch (Fig. 1). We decided to embolize the portovenous shunt to prevent overflow of the embolic agent into the systemic

K. Sofue (✉) · Y. Takeuchi · K. Shibamoto · Y. Arai
Department of Radiology, National Cancer Center Hospital, 5-1-1 Tsukiji, Chuo, Tokyo 104-0045, Japan
e-mail: keitarosofue@yahoo.co.jp

K. Sofue · K. Sugimoto · K. Sugimura
Department of Radiology, Kobe University, Graduate School of Medicine, Kobe, Japan

Fig. 1 Selective right posterior portogram with balloon occlusion revealed an intrahepatic portovenous shunt connecting the segment VII branches to the right hepatic venous branch (*arrow*)

Fig. 3 Direct portogram obtained after embolization of right portal vein revealed no residual flow in the right portal venous branch or intrahepatic portovenous shunt

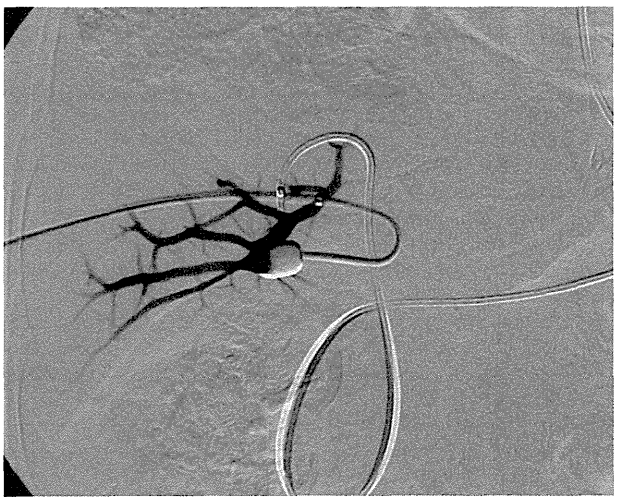

Fig. 2 Right posterior portogram with balloon occlusion after the infusion of 10 ml of 50 % glucose solution confirmed disappearance of the intrahepatic portovenous shunt

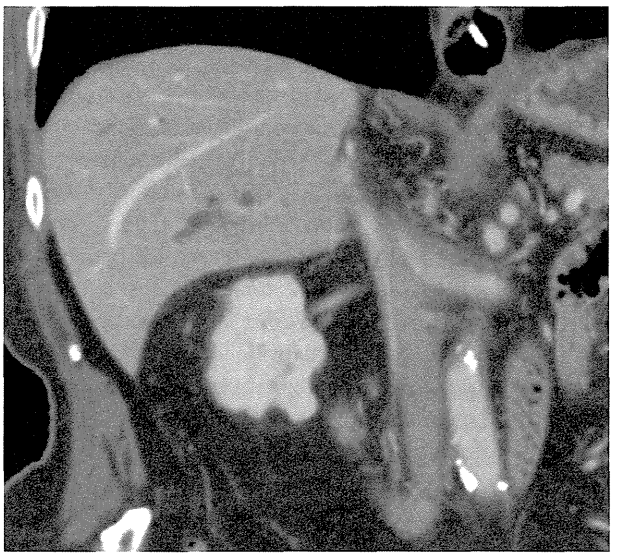

Fig. 4 Coronal image of contrast-enhanced computed tomography obtained 20 days after portal vein embolization shows sufficiently thrombosed right portal branches without right hepatic vein embolization

circulation and to occupy the right posterior branch of the portal vein with embolic agent exclusively.

First, we infused 10 ml of 50 % glucose solution from the catheter, keeping the balloon inflated. Repeated selective right posterior portography showed disappearance of the portovenous shunt (Fig. 2). We injected 5 ml of absolute ethanol to embolize the right posterior branch of the portal vein, and 6 ml of absolute ethanol with balloon occlusion to embolize the right anterior branch of the portal vein. Finally, post-embolization portography confirmed complete occlusion of the right portal branches (Fig. 3).

He was followed-up for 20 days after the procedure using computed tomography, and the left lobe of the liver became hypertrophic with a hypertrophy rate of 151.7 % without recanalization of right portal vein, right hepatic vein embolization, and unexpected pulmonary embolization (Fig. 4). He underwent extended right hepatectomy 24 days after the procedure, and his postoperative course was uneventful.

Discussion

Percutaneous transhepatic portal embolization (PTPE) is widely accepted as an effective method for inducing

atrophy of the embolized lobe to be resected and compensatory hypertrophy of the contralateral lobe [1, 2]. The technical considerations for PTPE are that the portal vein is securely occluded, stagnating the embolic agents such as liquid or microparticles, without recanalization and non-target embolization [1, 6].

An IPSVS is a rare vascular anomaly which communicates persistently between the portal vein and the hepatic vein [3]. Two theories have been proposed to explain the cause of IPSVSs: congenital origin, suggesting a persistent embryonic venous anastomosis; and acquired origin, suggesting the formation of a shunt following portal hypertension or trauma [3, 4]. Typical contrast-enhanced CT findings of IPSVS are a dilated portal branch directly communicating with the hepatic vein through a dilated venous aneurysm [7]. Treatment of IPSVSs should be considered for patients with symptoms of hepatic encephalopathy. However, the IPSVS must be occluded before the PTPE, because it may cause insufficient occlusion of the portal vein and unexpected embolization of the pulmonary artery due to overflow of the embolic agent through the shunt. The embolic agents used for IPSVS should be selected according to the shunt size and morphology. Coils, gelatin sponge, n-butyl cyanoacrylate, and an amplatzer vascular plug have all been used [3, 5, 8].

We decided to use 50 % glucose solution to occlude the small shunt in our patient. Previous reports proposed the embolic mechanism of 50 % glucose for patients with esophageal or gastric varices treated endoscopically, as the endothelial cells of the vessel are injured by its high osmolarity, blood flow stagnates, and thrombus formation [9, 10]. Several investigators have also reported the utility of hypertonic solution injected into the vessels directly during balloon-occluded retrograde transvenous obliteration and sclerotherapy of the varicose leg veins [11, 12]. The advantages of 50 % glucose are that it is easy to inject repeatedly without significant risk and it is less expensive than other embolic materials. We aimed to decrease the blood flow of the IPSVS, thereby allowing the injected absolute ethanol to occupy the portal vein sufficiently. This experiment was similar to that of the 50 % glucose solution infusion to occlude collateral vessels before the injection of ethanolamine oleate to treat gastric varices [11]. The shortcoming of 50 % glucose solution infusion would be that a large IPSVS is not occluded and remains after the injection, and embolization using coils or an amplatzer vascular plug may be required. An additional disadvantage is that injecting a large amount of the agent may induce hyperglycemia. Further experience or studies are warranted to clarify the embolic efficacy of 50 % glucose infusion for IPSVS, because this study is only case report and not fully supported theoretically.

In summary, we reported a case of percutaneous transhepatic portal embolization coexisting with an IPSVS, which was successfully occluded with an infusion of 50 % glucose solution. This is novel management for IPSVSs that are numerous, small, or torturous, and makes the accompanying procedures simpler, shorter, and less expensive, reducing the need for coils or an amplatzer vascular plug.

Conflict of interest Keitaro Sofue and his co-authors have no conflict of interest.

References

1. Madoff DC, Abdalla EK, Vauthey JN. Portal vein embolization in preparation for major hepatic resection: evolution of a new standard of care. J Vasc Interv Radiol. 2005;16:779–90.
2. Wakabayashi H, Okada S, Maeba T, Maeta H. Development of a de novo tumorous necrotic lesion in the liver after transcatheter arterial embolization combined with iodized oil infusion: report of a case. Surg Today. 1996;26:49–52.
3. Chevallier P, Oddo F, Souci J, Diaine B, Padovani B. Macroscopic intrahepatic portosystemic venous shunt: review of the literature and reclassification. J Radiol. 2001;81:597–604.
4. Park JH, Cha SH, Han JK, Han MC. Intrahepatic portosystemic venous shunt. AJR Am J Roentgenol. 1990;155:527–8.
5. Lee YJ, Shin BS, Lee IH, Ohm JY, Lee BS, Ahn M, et al. Intrahepatic portosystemic venous shunt: successful embolization using the Amplatzer Vascular Plug II. Korean J Radiol. 2012;13:827–31.
6. Di Stefano DR, de Baere T, Denys A, Hakime A, Gorin G, Gillet M, et al. Preoperative percutaneous portal vein embolization: evaluation of adverse events in 188 patients. Radiology. 2005;234:625–30.
7. Ito K, Fujita T, Shimizu A, Sasaki K, Tanabe M, Matsunaga N. Imaging findings of unusual intra- and extrahepatic portosystemic collaterals. Clin Radiol. 2009;64:200–7.
8. Yoshimatsu R, Takeuchi Y, Morishita H, Iida N, Okabe H, Yamagami T, et al. Successful embolisation of intrahepatic portosystemic venous shunt using coils and n-butyl cyanoacrylate through two approach routes. Br J Radiol. 2006;79:e162–5.
9. Chang KY, Wu CS, Chen PC. Prospective, randomized trial of hypertonic glucose water and sodium tetradecyl sulfate for gastric variceal bleeding in patients with advanced liver cirrhosis. Endoscopy. 1996;28:481–6.
10. Kuo MJ, Yeh HZ, Chen GH, Poon SK, Yang SS, Lien HC, et al. Improvement of tissue-adhesive obliteration of bleeding gastric varices using adjuvant hypertonic glucose injection: a prospective randomized trial. Endoscopy. 2007;39:487–91.
11. Yamagami T, Kato T, Hirota T, Yoshimatsu R, Matsumoto T, Nishimura T. Infusion of 50 % glucose solution before injection of ethanolamine oleate during balloon-occluded retrograde transvenous obliteration. Australas Radiol. 2007;51:334–8.
12. Le Baleur A, Bourgeois A, Gillot C, Pillot P, Bellagha I, Frileux C. Per-operative multi-sclerosis using 66 % glucose. Treatment of choice and best prevention of pigmentations of venous origin. Phlebologie. 1983;36:349–52.

J Gastroenterol (2014) 49:932–940
DOI 10.1007/s00535-013-0853-7

The Japanese Society of Gastroenterology

ORIGINAL ARTICLE—LIVER, PANCREAS, AND BILIARY TRACT

Efficacy of sorafenib in patients with hepatocellular carcinoma refractory to transcatheter arterial chemoembolization

Masafumi Ikeda · Shuichi Mitsunaga · Satoshi Shimizu · Izumi Ohno · Hideaki Takahashi · Hiroyuki Okuyama · Akiko Kuwahara · Shunsuke Kondo · Chigusa Morizane · Hideki Ueno · Mitsuo Satake · Yasuaki Arai · Takuji Okusaka

Received: 5 March 2013 / Accepted: 9 June 2013 / Published online: 23 June 2013

Abstract
Background The efficacy of sorafenib for hepatocellular carcinoma (HCC) patients refractory to transcatheter arterial chemoembolization (TACE) has not yet been clarified. We investigated the efficacy of sorafenib in HCC patients who were refractory to TACE (sorafenib group) and retrospectively compared the results with those of patients treated with hepatic arterial infusion chemotherapy using cisplatin (cisplatin group).
Methods We evaluated the anti-tumor effect, the time to progression, and the overall survival in 48 patients in the sorafenib group and 66 patients in the cisplatin group.
Results The disease control rate to sorafenib was 60.4 %, the median time to progression was 3.9 months, and the median survival time was 16.4 months in patients who were refractory to TACE. When compared with the cisplatin group, significant differences in the patient characteristics were not observed between the two groups with the exception of patient age; however, the disease control rate (cisplatin group 28.8 %, $P = 0.001$), time to progression (cisplatin group: median 2.0 months, hazard ratio 0.44, $P < 0.01$), and overall survival (cisplatin group: median 8.6 months, hazard ratio 0.57, $P < 0.001$) were significantly superior in the sorafenib group. The multivariate analysis also showed the sorafenib treatment to be the most significant factor contributing to prolongation of time to progression and overall survival.
Conclusions Sorafenib showed favorable treatment results in patients refractory to TACE. When compared with hepatic arterial infusion chemotherapy using cisplatin, sorafenib demonstrated a significantly higher disease control rate, a longer time to progression and increased overall survival.

Keywords Hepatocellular carcinoma · Sorafenib · Cisplatin · Chemotherapy · Hepatic arterial infusion chemotherapy

Introduction

Hepatocellular carcinoma (HCC) is one of the most common malignancies worldwide. HCC is highly prevalent in African and Asian countries, and its incidence has recently been increasing in western countries [1, 2]. For patients with unresectable HCC who are not candidates for curative treatments, such as resection, transplantation, or local ablation, transcatheter arterial chemoembolization (TACE) is the main therapeutic option [1, 2]. A clear survival benefit for patients with unresectable HCC who are treated with TACE has been shown in several randomized controlled trials and a meta-analysis [3, 4]. Chemotherapy has been recognized as a palliative treatment option for patients with highly advanced HCC in whom TACE is not indicated.

Sorafenib is a multikinase inhibitor of Raf kinase, which is involved in cancer cell proliferation, as well as vascular

M. Ikeda (✉) · S. Mitsunaga · S. Shimizu · I. Ohno · H. Takahashi · H. Okuyama · A. Kuwahara
Division of Hepatobiliary and Pancreatic Oncology, National Cancer Center Hospital East, 6-5-1 Kashiwanoha, Kashiwa, Chiba 277-8577, Japan
e-mail: masikeda@east.ncc.go.jp

S. Kondo · C. Morizane · H. Ueno · T. Okusaka
Hepatobiliary and Pancreatic Oncology Division, National Cancer Center Hospital, Tokyo, Japan

M. Satake
Division of Diagnostic Radiology, National Cancer Center Hospital East, Kashiwa, Japan

Y. Arai
Department of Diagnostic Radiology, National Cancer Center Hospital, Tokyo, Japan